Contents lists available at ScienceDirect

Computational and Structural Biotechnology Journal

Research Article

Cluster-based radiomics reveal spatial heterogeneity of bevacizumab response for treatment of radiotherapy-induced cerebral necrosis

Hong Qi Tan [a,1], Jinhua Cai [b,c,d,1], Shi Hui Tay [e,1], Adelene Y.L. Sim [e], Luo Huang [f], Melvin L.K. Chua [a,e,g,2,*], Yamei Tang [b,c,d,2,**]

[a] Division of Radiation Oncology, National Cancer Centre Singapore, Singapore
[b] Department of Neurology, Sun Yat-sen Memorial Hospital, Sun Yat-sen University, Guangzhou, People's Republic of China
[c] Guangdong Provincial Key Laboratory of Malignant Tumor Epigenetics and Gene Regulation, Sun Yat-sen Memorial Hospital, Sun Yat-sen University, Guangzhou, People's Republic of China
[d] Guangdong Provincial Key Laboratory of Brain Function and Disease, Zhongshan School of Medicine, Sun Yat-sen University, Guangzhou, People's Republic of China
[e] Division of Medical Sciences, National Cancer Centre Singapore, Singapore
[f] Department of Radiation Oncology, Chongqing University Cancer Hospital, People's Republic of China
[g] Oncology Academic Programme, Duke-NUS Medical School, Singapore

ARTICLE INFO

ABSTRACT

Background: Bevacizumab is used in the treatment of radiation necrosis (RN), which is a debilitating toxicity following head and neck radiotherapy. However, there is no biomarker to predict if a patient would respond to bevacizumab.

Purpose: We aimed to develop a cluster-based radiomics approach to characterize the spatial heterogeneity of RN and map their responses to bevacizumab.

Methods: 118 consecutive nasopharyngeal carcinoma patients diagnosed with RN were enrolled. We divided 152 lesions from the patients into 101 for training, and 51 for validation. We extracted voxel-level radiomics features from each lesion segmented on T1-weighted+contrast and T2 FLAIR sequences of pre- and post-bevacizumab magnetic resonance images, followed by a three-step analysis involving individual- and population-level clustering, before delta-radiomics to derive five radiomics clusters within the lesions. We tested the association of each cluster with response to bevacizumab and developed a clinico-radiomics model using clinical predictors and cluster-specific features.

Results: 71 (70.3%) and 34 (66.7%) lesions had responded to bevacizumab in the training and validation datasets, respectively. Two radiomics clusters were spatially mapped to the edema region, and the volume changes were significantly associated with bevacizumab response (OR:11.12 [95% CI: 2.54–73.47], $P = 0.004$; and 1.63 [1.07–2.78], $P = 0.042$). The combined clinico-radiomics model based on textural features extracted from the most significant cluster improved the prediction of bevacizumab response, compared with a clinical-only model (AUC:0.755 [0.645–0.865] to 0.852 [0.764–0.940], training; 0.708 [0.554–0.861] to 0.816 [0.699–0.933], validation).

Conclusion: Our radiomics approach yielded intralesional resolution, enabling a more refined feature selection for predicting bevacizumab efficacy in the treatment of RN.

---

* Correspondence to: Department of Head and Neck and Thoracic Cancers, Division of Radiation Oncology, National Cancer Centre Singapore, 11 Hospital Crescent, 169610, Singapore.
** Correspondence to: Department of Neurology, Sun Yat-sen Memorial Hospital, Sun Yat-sen University, 107 Yan Jiang Xi Road, Guangzhou, Guangdong Province, People's Republic of China.
E-mail addresses: gmsclkm@nus.edu.sg (M.L.K. Chua), tangym@mail.sysu.edu.cn (Y. Tang).
[1] Co-first authors.
[2] Co-senior authors.
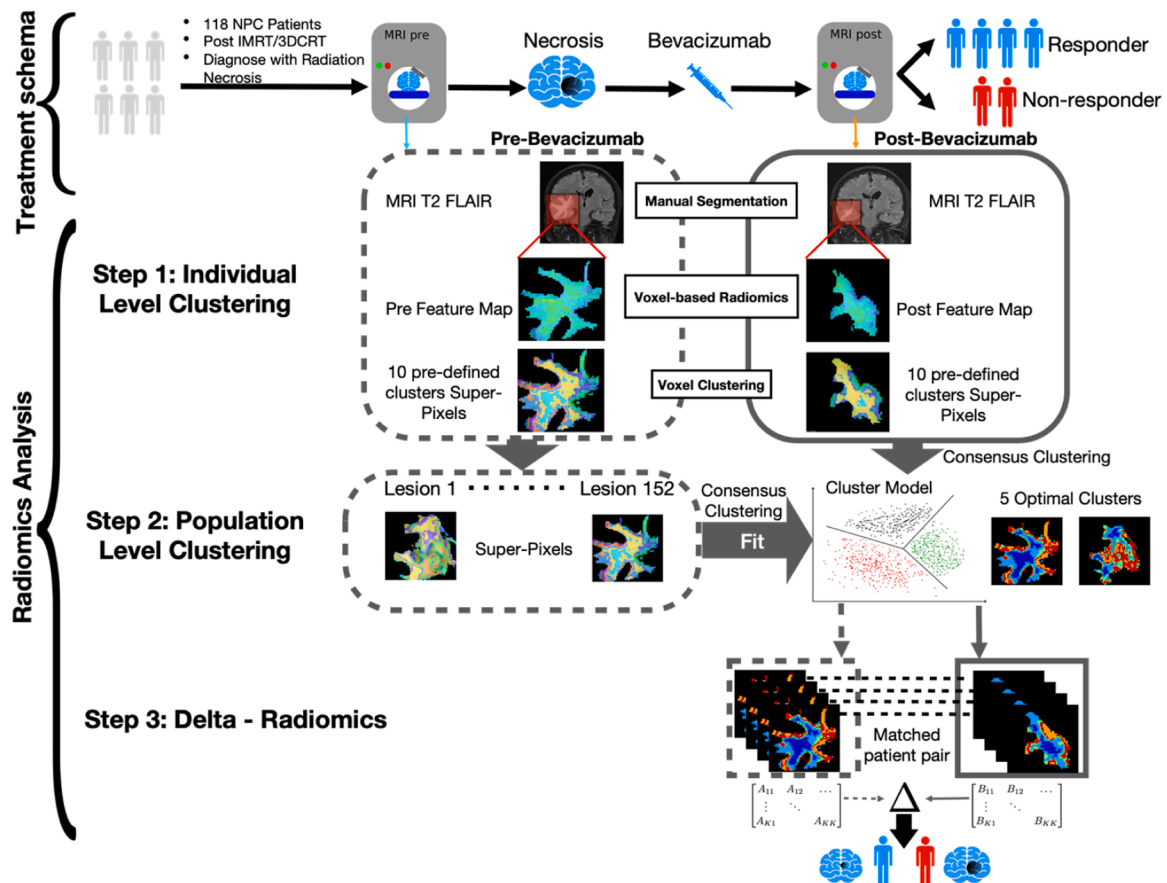
Fig. 1. An overview of the cluster-based radiomics analysis pipeline. Pre- and post-treatment T2 FLAIR MR images of 152 RN lesions were manually segmented, followed by feature extraction at the voxel level for all the lesions. The first step involved individual-level clustering, where K-means clustering using 10 fixed clusters was applied to all the textural feature vectors in the voxel of each lesion. The second phase involved population-level clustering, where K-means clustering was applied to the textural feature centroid vectors from all the lesions in the training dataset. The last step would be delta radiomics to correlate any changes in the radiomics clusters following treatment to bevacizumab response.

1. Introduction

Radiotherapy is an integral treatment modality in the management of head and neck cancers [1,2]. Whilst effective, radiotherapy in the head and neck region can impose substantial acute and delayed toxicities due to the sensitivity of normal tissues, such as the salivary glands, and neurological structures, including the temporal lobes, brainstem, cranial nerves, etc., in this anatomical region [3–5]. Depending on the tumor location, some delayed post-radiotherapy complications are unavoidable, such as the onset of cerebral radiation necrosis (RN) in the temporal lobes that affects 3–24% of nasopharyngeal carcinoma (NPC) patients following radiotherapy, especially for those with base of skull and intracranial involvement [6–8].

RN is conventionally treated with corticosteroid, which is associated with a broad spectrum of toxicities, including Cushing's and other metabolic syndromes, gastric discomfort, and myopathy [9]. However, only about 35% of RN patients derive a clinical benefit following corticosteroid [10]. Bevacizumab on the other hand is a humanized monoclonal antibody against vascular endothelial growth factor (VEGF), and it has demonstrated activity in the treatment of RN. Xu *et al.* conducted a randomized trial demonstrating that bevacizumab was able to yield a substantial radiological response in RN lesions of up to 60%, corresponding to a clinical improvement in 66% of patients [11]. Despite the pronounced radiological and clinical benefits, 34% of the patients in this trial had failed to respond to bevacizumab [11], notwithstanding the potential risk of bleeding with bevacizumab in NPC patients post-radiotherapy [12]. These reasons provide the clinical rationale to develop predictive models to identify RN patients who would derive a benefit from bevacizumab.

Radiomics extracts multi-dimensional quantitative information from medical images of different modalities to build models for guiding treatment decisions [13,14]. In recent times, there has been much interest in applying radiomics in oncology for a variety of purposes, as it is non-invasive and is preferred over deep-learning when dealing with small sample sizes [15]. Given the high dimensionality of radiomics features, it is often necessary to employ appropriate feature selection methods to mitigate computational complexity and model overfitting. Our prior work applied the conventional radiomics approach to develop and validate a radiomics model that was superior to clinical factors for predicting bevacizumab responses in RN patients [16]. However, our model was limited by the fact that it was designed to predict binarized bevacizumab responses (responder versus non-responder) but overlooked the intralesional variation of bevacizumab response. Similar to most radiomics models, it is unable to resolve spatial heterogeneity within a volume of interest (VOI) or provide any biological relevance to the selected features, thus affecting its interpretability.

To address these issues, we investigated a novel radiomics pipeline by integrating an unsupervised clustering algorithm with voxel-level and delta radiomics to derive spatially distinct radiomics clusters, which were then tested for their respective associations with bevacizumab response. Using our method, we found that only certain high-resolution radiomics features that were correlated with specific radiological subregions of the RN lesion – as opposed to features that aggregate properties of the whole lesion – were associated with

Table 1
Clinical characteristics of the patients.

Variables	Training (N = 77)	Validation (N = 41)	P
Age (years)	50 (43–56)	44 (39–52)	0.016
Sex			
Male	56 (72.7)	32 (78.0)	0.682
Female	21 (27.3)	9 (22.0)	
LENT/SOMA			
Grade 1	11 (14.3)	10 (24.4)	0.043
Grade 2	18 (23.4)	16 (39.0)	
Grade 3	31 (40.2)	12 (29.3)	
Grade 4	17 (22.1)	3 (7.3)	
MoCA	24.0 (23.0–27.0)	24.0 (22.0–27.0)	0.535
QOL	58.3 (57.1–61.7)	58.3 (53.2–63.2)	0.669
IRB (months)	49.1 (31.9–69.0)	38.8 (21.0–75.1)	0.079
IBT (months)	3.7 (0.6–12.6)	3.3 (1.2–6.2)	0.832
D_{max} to the brain (Gy)	70.0 (68.0–72.0)	70.0 (68.0–70.0)	0.180
Radiation approach			
Conventional radiotherapy	38 (49.4)	15 (36.6)	0.257
IMRT	39 (50.6)	26 (63.4)	
Laterality of RN lesions			
Unilateral	53 (68.8)	31 (75.6)	0.575
Bilateral	24 (31.2)	10 (24.4)	
Pre-bevacizumab lesion volume[a] (cm^3)	25.0 (12.8–65.1)	21.5 (9.8–45.1)	0.279
Decrease in lesion volume, median[a] (%)	56.2 (12.9–80.3)	54.7 (12.9–86.7)	0.786
Documented response to bevacizumab			
Non-responder (NR)	30 (29.7)	17 (33.3)	0.786
Responder (R)	71 (70.3)	34 (66.7)	

The data are shown as the number (percentage) or median (interquartile range). Abbreviations: IBT, interval between diagnosis of brain necrosis and treatment with bevacizumab; D_{max}, maximum radiation dose; IRB, interval between radiotherapy and diagnosis of brain necrosis; IMRT, intensity-modulated radiation therapy; LENT/SOMA, Late Effects of Normal Tissue Subjective, Objective, Management
[a] Each individual brain lesion was considered as a subject to be measured in these clinical variables.

bevacizumab response in our cohort of NPC patients with RN post-radiotherapy. We utilized these radiomics features in conjunction with our clinical predictors to construct a clinico-radiomics model. The combined model not only demonstrated enhanced performance compared to either clinical or radiomics models used independently but also effectively addressed spatial heterogeneity, a component that was absent in previous radiomics workflow.

2. Materials and methods

2.1. Patient cohort and treatment

This retrospective study was approved by the institutional review board of Sun Yat-sen Memorial Hospital and conducted in accordance with the Declaration of Helsinki. Written informed consent was obtained from all patients. We included patients with NPC that developed cerebral necrosis after radiotherapy to minimize the likelihood of a misdiagnosis of a tumor recurrence. Moreover, brain metastasis recurrence is a rare clinical phenomenon in NPC [17]. The inclusion and exclusion criteria are outlined in the Supplementary methods. 118 consecutive patients who had been diagnosed with RN and treated with bevacizumab between July 2012 and March 2019 at the Sun Yat-sen Memorial Hospital were enrolled in this study. These patients were sourced from the same cohort as our previous study [16]. Of them, 77 patients with 101 brain lesions were assigned to the training dataset, while 41 patients with 51 brain lesions were assigned to the validation dataset, as

previously described [16]. The Mann-Whitney U test and Chi-Square test were used to examine the statistical differences in clinical variables between the two datasets. The diagnosis of RN was made based on the consensus opinions of both neurologists and radiologists [17–19].

2.2. Cluster-based MRI radiomics pipeline

An overview of the cluster-based radiomics pipeline that was used to investigate the spatiotemporal association of the radiomics clusters with response to bevacizumab is shown in Fig. 1.

2.2.1. MR image segmentation and radiomics feature extraction

Manual segmentations of the edema and necrotic regions of each VOI were performed on pre- and post-treatment MRI scans using the 3D Slicer software (version 4.9.0), as previously described [16]. The images and segmentations were first interpolated to yield an isotropic voxel resolution of 1 mm using linear interpolation. The voxel values were then standardized in each lesion to ensure a similar voxel value dynamic range across lesions. Radiomics features were extracted from each voxel within the segmented VOI on T2-Flair sequence using *Pyradiomics 2.2.0*, which is compliant with the biomarker standardization initiative [20]. First-order features were omitted because the image voxel value histogram and absolute value varied greatly between patients even for the same anatomical structure. The omission of these features was to introduce robustness to account for variations in MR scanner and acquisition protocols in the model. Furthermore, since the clustering performance deteriorates rapidly with increased feature dimension [21, 22], only a single type of textural feature was selected. Focusing solely on the GLCM textural features, we extracted a total of 24 gray-level co-occurrence matrix (GLCM) feature maps. This was further reduced to 10 GLCM feature maps based on the robustness to Gaussian noise addition in the small kernel. At this stage, each voxel had a 10-dimensional feature vector representative of local texture.

#### 2.2.2. Individual-level clustering

K-means clustering based on 10 pre-defined number of clusters was applied on pre- and post-treatment images to over-segment the VOI, resulting in a superpixel. Specifically, the feature vectors of all the voxels in the lesion were inputted into the clustering algorithm to assign a cluster label to each voxel. The 10 centroid vectors of each lesion were recorded to represent the textural feature vector of RN lesion.

2.2.3. Population-level clustering

Clustering at the population-level, where all the centroid vectors from the pre-treatment images of the RN lesions were aggregated at the cohort level to derive the final cluster heatmap. Ensemble clustering method was used to ensure robust clustering results. 130 ensembles were applied, and K-means clustering was used in each ensemble with a different bootstrapped sample. The optimal number of clusters was defined using the elbow method with ΔK metric [23]. The output of the ensemble clustering was the final cluster heatmap for the lesion of each patient. Then, the cluster heatmaps in the post-treatment images were obtained using the centroids defined from the pre-treatment images. The 3D heatmap provided an intuitive visualization of the heterogeneity within the VOI. Finally, delta radiomics was performed to link the change in the pre- and post-treatment radiomics clusters to treatment response.

2.3. Definition of radiological subregions and spatial mapping of radiomics clusters within the RN VOI

To perform spatial correlation analyses, we delineated the RN VOI into 3 distinct subregions, namely necrosis, edema, and boundary. The necrotic region was manually contoured by observing the enhanced lesion on the T1w+C sequence, while the whole lesion comprising of the edema and necrotic subregions was contoured based on the T2-FLAIR
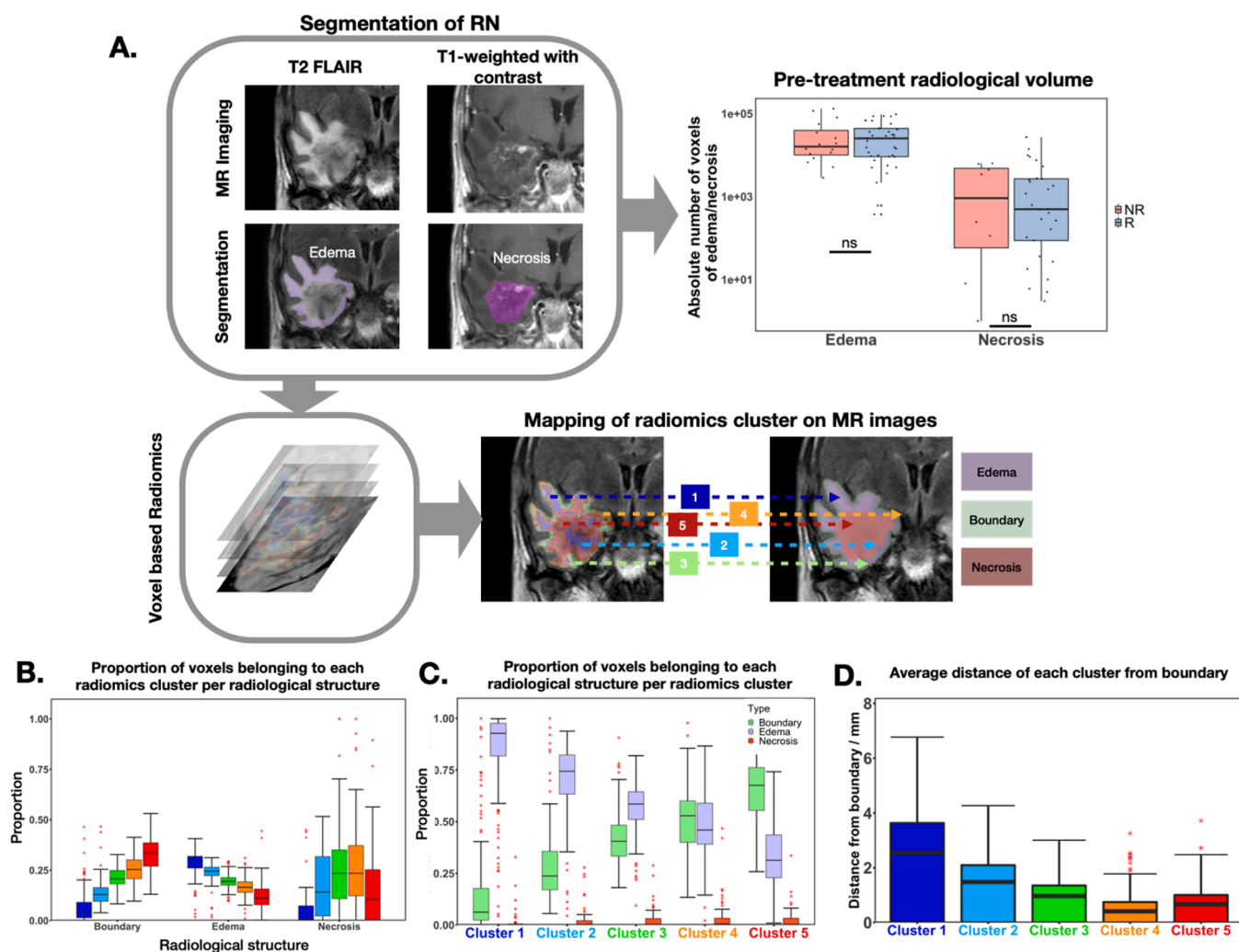
Fig. 2. Mapping of radiomics clusters to radiological subregions. (A) Workflow for spatial mapping of radiomics clusters with the radiological subregions. T2 FLAIR and T1-weighted with gadolinium contrast sequences were used for the manual segmentation of edema and necrosis, respectively. Pre-treatment volumes of edema and necrosis for the training and testing datasets are shown in the adjacent box plots. (B) Composition of edema, necrosis, and boundary by the different radiomics clusters. (C) Proportion of voxels of each radiomics cluster localized to boundary, edema, and necrosis. (D) Median of the average distances of the radiomics clusters from the boundary of the 152 RN lesions.

sequence. The edema subregion was then obtained by the Boolean subtraction of the necrosis volume from the whole VOI. The boundary subregion was defined by a fixed margin of one voxel around the VOI.

The assignment of the radiomics clusters to the radiological subregions was then based on calculating the proportion of voxels of each radiomics cluster that resided within each radiological subregion. The Kruskal-Wallis test was used to determine if there were statistically significant differences across the clusters. Additionally, the distance of the radiomics cluster from the boundary was quantified for each RN lesion. The distance was defined as the mean of the shortest two-dimensional Euclidean distance of all the voxels within a particular cluster from the boundary.

2.4. Differential response of radiomics clusters to bevacizumab

Pre- and post-treatment MR images were co-registered, so that each voxel in the pre-treatment MR image was mapped to the corresponding radiological voxel in the post-treatment MR image. Rigid transformation was carried out using *Plastimatch v1.8.0* [18]. The association between the decrease in radiomics cluster size, based on the absolute number of voxels, and bevacizumab response was determined using the aggregated volume change and univariable analysis.

2.5. Response prediction with cluster-specific features

Hand-crafted features shown in Table S1 were extracted from the cluster heatmap of each RN VOI of the pre-treatment MR images. In addition to the aggregate and fractional cluster volume features of all clusters, textural features from the cluster that was most significantly associated with bevacizumab response were included for model building. Fig. S1 illustrates the features extracted from the clusters to build the model. Three different models were constructed, namely radiomics, clinical and combined model. The radiomics-only model utilized a combination of the LASSO algorithm and a bagging strategy to predict bevacizumab response [19]. The LASSO algorithm was used to handle the issue of correlated features, and the bagging strategy was used to improve the generalizability of the model. 100 ensembles were used in the Bagging algorithm and λ value corresponding to the minimum point of the binomial deviance curve was used for LASSO in each ensemble. A variable importance plot was produced to rank the cluster-specific features driving the prediction. Two significant clinical predictors, ascertained by univariate analysis [16] – 1) time interval between radiotherapy and diagnosis of RN (OR=0.976 [95% CI: 0.952–0.995], $P = 0.025$), and 2) time interval between diagnosis of RN and treatment with bevacizumab (OR=0.984 [95% CI: 0.971–0.995], $P = 0.008$), were
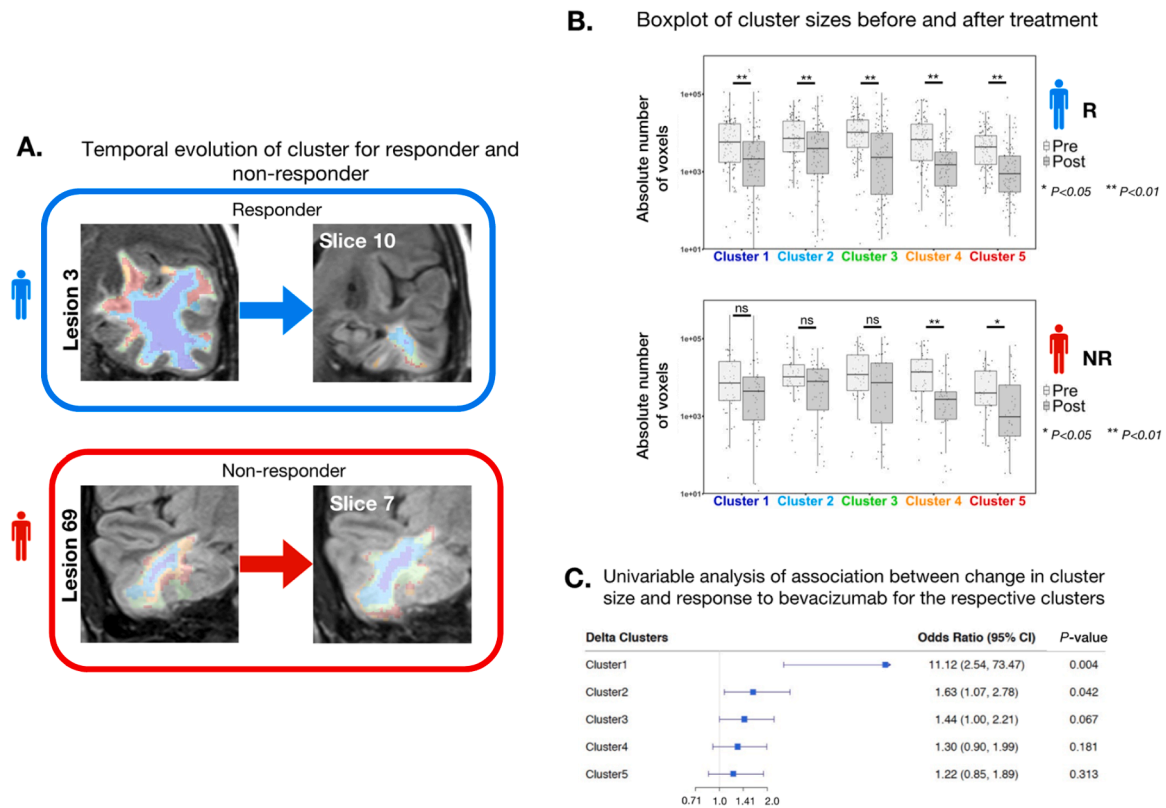
Fig. 3. Cluster evolution between pre- and post-treatment MR scans. (A) Cluster evolution for a responding RN lesion (top), and a non-responding lesion (bottom). (B) Comparison of the cluster sizes before and after treatment for responders and non-responders. (C) Forest plot showing the odds ratios from the univariable analysis of associations between change in cluster size and bevacizumab response for the respective clusters.

used to construct the clinical-only model. Finally, the predicted probability from the Bagging LASSO algorithm was used as a single "radiomics score" and combined with the two significant clinical predictors to form the final set of indices for the combined model. The clinical-only and combined models were both conventional logistic regression models. The performance of the combined model was compared with the radiomics-only and clinical-only models using area under the curve (AUC) of the receiver operating curves (ROCs) and calibration curves generated from the predicted probabilities.

2.6. Statistical analyses and toolboxes

All statistical tests were performed using the R statistical software (version 3.4.2; R Foundation for Statistical Computing). The Scikit-Learn v0.20.3 module was used to perform K-means clustering. The Cluster_-Ensembles v1.16 module was used for ensemble clustering. Bagging-LASSO was performed using the SparseLearner v1.02 module in RStudio. The ROC curve and 95% confidence interval were determined using the ROCR v1.0–7 package, and the calibration curves were generated using PredictABEL v1.2–4 package in R. A two-sided p-value of < 0.05 was considered statistically significant.

3. Results

3.1. Patient cohort and response to bevacizumab

The clinical characteristics of the study cohort were previously summarized [16], as shown in Table 1. There were no significant differences in clinical parameters between the training and validation datasets, except age ($P = 0.016$), and late effects of normal tissue subjective ($P = 0.043$). Overall, 71 (70.3%) and 34 (66.7%) lesions in the training and validation datasets, respectively, manifested radiological

responses to bevacizumab. The corresponding median percentages reduction of RN VOI were 71.8% (IQR: 54.7–87.5) in responders, and 13.2% (IQR: 7.98–21.4) in non-responders.

3.2. Spatial mapping of radiomics clusters to radiological subregions within the RN lesion

Using our three-step radiomics analysis, we derived five optimal radiomics clusters (Fig. S2), where each cluster is represented by a different color (Fig. 1). Next, we attempted to overlay the radiomics clusters over each pre-treatment RN VOI, mapping them to the three radiological subregions – necrosis, edema, and boundary, as aforementioned (Fig. 2A). We did not observe a difference in pre-treatment volumes of the necrosis and edema subregions between responders and non-responders (Fig. 2A; $P = 0.5112$, necrosis, $P = 0.3003$ for edema). We also found that each radiomics cluster was differentially associated with edema, necrosis, and boundary. Based on the cluster assignment of voxels within each radiological subregion, most of the boundary subregion was comprised of cluster 5 (red), while cluster 1 (blue) was the dominant cluster within the edema subregion. Necrosis was mostly comprised of clusters 3 (green) and 4 (orange) (Fig. 2B). This finding was corroborated by Fig. 2C, which showed the proportion of each radiological subregion within the radiomics clusters; here, we showed that the boundary and edema subregions were inversely associated with the radiomics clusters, suggesting that these clusters represent a gradual change in texture. The Kruskal-Wallis test showed significant differences in the proportions of edema, boundary and necrosis across the five clusters, with $P < 0.001$ for edema and boundary, and $P = 0.0395$ for necrosis. The distances of the respective radiomics clusters from the boundary were also derived; clusters 4 (orange) and 5 (red) had smaller median distances of 0.411 mm (IQR=0.766 mm) and 0.671 mm (IQR=1.03 mm), respectively, from the boundary, compared with the
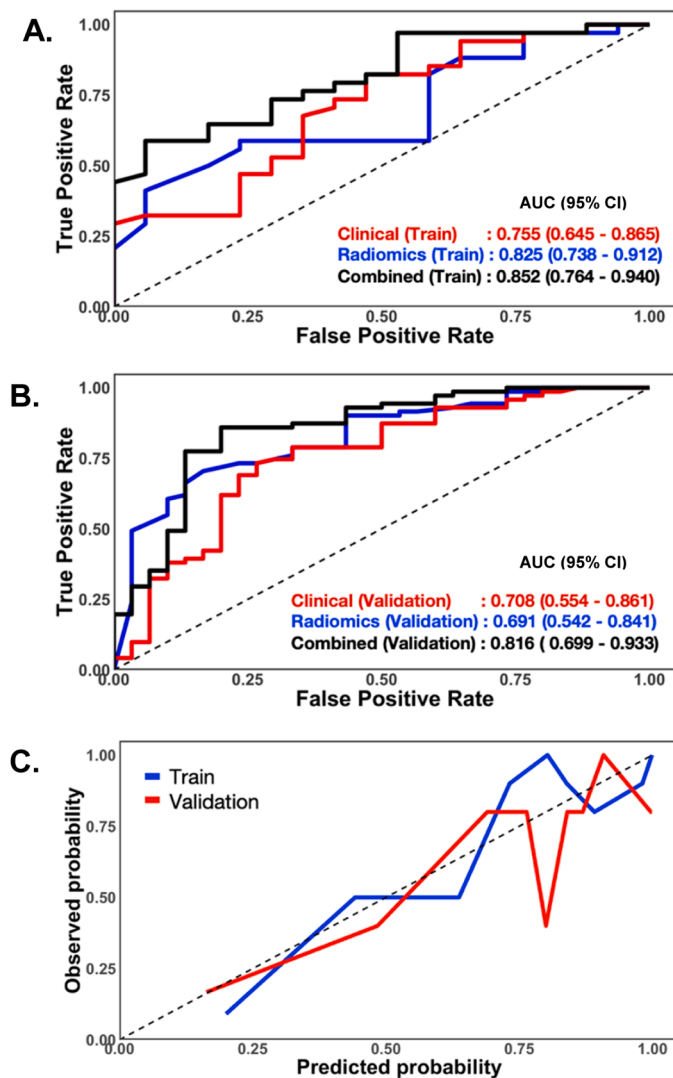
Fig. 4. Prediction of bevacizumab using cluster-derived radiomics features. (A, B) ROC curves comparing the clinical, radiomics, and combined clinico-radiomics models for training and validation datasets, respectively. (C) Calibration curves of the training and validation datasets.

other clusters (Fig. 2D).

3.3. Temporal evolution of the radiomics clusters between responders and non-responders

We reconstructed the cluster heatmaps on the post-treatment MR images to track the temporal evolution of the radiomics clusters in response to bevacizumab. Examples of the radiomics cluster evolution in a responder and non-responder are illustrated in Fig. 3A. Expectedly, the responder showed an overall reduction of the RN VOI and cluster 1 (blue), which is the dominant radiomics cluster within edema. In contrast, the non-responder showed minimal change for both RN VOI and cluster 1. Fig. 3B shows the cluster sizes before and after bevacizumab in responding and non-responding lesions. The former showed a significant reduction in volume for all the radiomics clusters, while the latter showed a non-significant decrease in cluster 1 (blue), cluster 2 (cyan), and cluster 3 (green), but a significant decrease in clusters 4 (orange) and 5 (red) volumes. Univariable tests of association between change in cluster size and response to bevacizumab for the respective clusters are presented in Fig. 3C. Among them, only the decrease in volumes of clusters 1 (blue) and 2 (light blue) showed significant

associations with bevacizumab response, with the odds ratios (*OR*) of 11.12 (95% confidence interval [CI]: 2.54–73.47) for cluster 1 and 1.63 (95%CI, 1.07–2.78) for cluster 2.

3.4. Prediction of response with cluster-specific radiomics features

Finally, we built a radiomics model based on the features defined in Table S1, which were extracted from the clusters in pre-treatment MR images to predict bevacizumab response. Since the change in volume of cluster 1 (blue) was identified to be most strongly associated with response to bevacizumab, we hypothesized that the textural features in cluster 1 would be the best predictors of bevacizumab response. In total, 30 cluster-specific features were selected using the bagging LASSO model; the variable importance plot is shown in Fig. S3. The results of the discriminatory ability of the radiomics, clinical and combined models in the training and validation datasets can be interpreted from the ROC curves in Figs. 4A and B, respectively. The combined clinico-radiomics model was superior to the clinical-only model, improving the AUC from 0.755 (95% CI, 0.645–0.865) to 0.852 (95%CI, 0.764–0.940) in the training, and from 0.708 (95%CI, 0.554–0.861) to 0.816 (95%CI, 0.699–0.933) in the validation datasets. The results of the calibrations for both training and testing datasets are shown in Fig. 4C. Both datasets showed non-significant statistics with Hosmer-Lemeshow tests ($P = 0.344$ for training, and $P = 0.331$ for validation), indicating no deviation between the logistic model and the perfect prediction. Overall, these results showed that features derived from specific radiomics clusters within the RN VOI could yield a well-calibrated model for predicting bevacizumab response.

4. Discussion

The past few years have witnessed a peak in interest in adopting radiomics for a variety of clinical applications, including the development of models to prognosticate survival in cancer patients, predict specific genotypes of cancers, and adapt treatment [24–26]. While the results are encouraging, the field has remained apprehensive in transitioning these models to the clinics, partly because of concerns regarding the explainability of these models. Most conventional radiomics models, including our previous model [16], were built using a series of single textural feature vectors extracted from a VOI. These radiomics approaches lack spatial resolution characterization and assume that a single feature vector represents the textural morphology of the whole 3D structure, thus prompting cynicisms regarding the reliability and reproducibility of these outputs to variations in image acquisition and VOI segmentation [16,27–29]. The interpretation of the single feature vector becomes challenging when dealing with segmentation comprising multiple distinct and heterogeneous regions, making it difficult to identify specific regions within the lesion that demonstrate significant treatment response. Moreover, textural features extracted from the entire lesion may encompass irrelevant features, potentially resulting in model overfitting. Consequently, the biological relevance leading to the predictive outcome remained elusive and could not be attributed to any influencing factor. To address the limitations of conventional volume-based radiomics models, here, we devised a novel cluster-based radiomics approach to provide spatial resolution of the textural features that could be associated with the response of RN lesions to bevacizumab treatment (Fig. 5). Specifically, we characterized the spatial heterogeneity of the lesion, which yielded multiple regions with diverse texture characteristics, enabling the identification of specific regions that demonstrate a significant treatment response. Furthermore, we selectively included textural features from the region of the lesion that demonstrated the strongest association with treatment response for model building. This targeted approach enhanced the model's feature relevance by focusing on the most informative region for predicting treatment response. We built this idea upon a voxel-level radiomics tool that was available in *PyRadiomics* [24,30]. We first derived a heatmap

Comparison of Conventional Volume-Based vs Cluster-Based Radiomics Pipelines
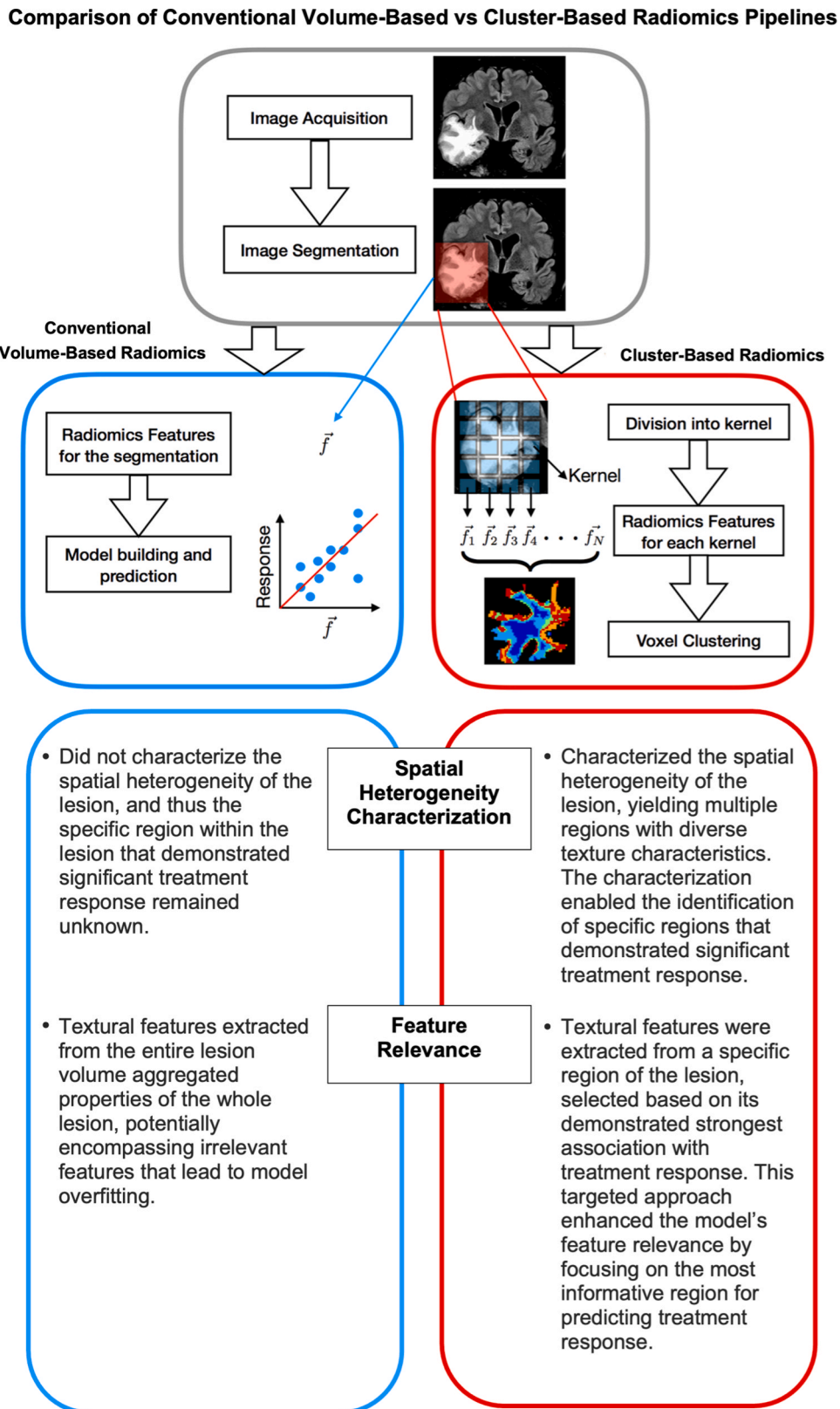
Fig. 5. A comparison of the conventional volume-based and cluster-based radiomics analyses. The conventional volume-based radiomics approach extracts a single radiomics feature vector per image segmentation, while the cluster-based radiomics approach extracts multiple feature heatmaps per segmentation. K-means clustering is performed on all the feature vectors in each voxel of the VOI to break down the VOI into multiple textural clusters for information on spatial heterogeneity.

using K-means clustering to visualize the radiomics textural clusters within the RN lesion, which were then spatially mapped to the radiological subregions. Each of the five derived radiomics clusters possesses unique texture characteristics with significantly different proportions of edema, necrosis, and boundary. We were subsequently able to determine the radiomics clusters that showed the largest delta pre- and post-treatment, which coupled with spatial-level information, revealed the intralesional variation of response to bevacizumab. We proceeded to show that the volume features extracted from all the clusters, along with textural features from the "significant" cluster (cluster 1), effectively captured intratumor heterogeneity and improved the prediction of bevacizumab response when the radiomics model was added to the clinical model. As a notable improvement over our previous model [16], we provided feature relevance of our radiomics model by consideration of spatial heterogeneity of intralesional response to bevacizumab, and incorporated textural features that were strongly associated with region-specific response in the model. Overall, our cluster-based radiomics approach revealed the correlation of the radiomics features with known radio-anatomical characteristics, and thus added a layer of biological relevance to the radiomics model, leading to an improved understanding of the final combined model.

Bevacizumab has been investigated for the treatment of RN on the rationale that abnormal vasculogenesis, induced due to hypoxic changes to the microenvironment post-radiation, thereby resulting in increased vessel permeability and consequential interstitial tissue edema and damage, is the dominant mechanism underpinning RN [27]. Radiological responses to bevacizumab are thus characterized by an initial reduction of edema, followed by ensuing resolution of the necrosis [28, 29,31]. In our analyses of 152 RN lesions, we found that among the five radiomics clusters, cluster 1 was most closely associated with edema, with 92.6% of the voxels localized within this radiological subregion. Therefore, it was not unexpected that radiomics features, including the change in the size, of cluster 1 showed the strongest association with bevacizumab response (*OR* of 11.12). From this improved radiomics workflow, we have demonstrated that by adding a layer of spatial radiomics, one could enhance the explainability of the radiomics analytical output, especially when the findings concur with underlying biological mechanisms.

The ability to visualize radiomics clusters within a VOI aids in the interpretation of any association between a radiomics feature/model and the clinical outcome of interest. For instance, the existence of cluster 1 within edema, through visual inspection, could explain why radiomics features within this cluster carried the highest weightage in the eventual prediction model (see variable importance plot – Fig. S3). This visualization is also analogous to the grad-CAM [32] method in the convolutional neural network (CNN) for highlighting important regions in the image that are contributing to a prediction. The availability of such tools is crucial for the interpretation of radiomics models, as it may lower the barrier to clinical implementation. Besides, such tools can enable the investigation of specific subregions within an image, allowing for a more focused analysis, especially in cases where different regions exhibit diverse characteristics or response to treatment.

Despite the encouraging results of this new radiomics approach, there are some limitations to this study. Firstly, the small sample size of our study could have adversely influenced the clustering results, and we lacked an external dataset to determine the generalizability of our algorithm. We plan to extend our work to include other tumor types, and in larger cohorts. Secondly, our final bevacizumab response model was constructed based on pre-treatment MR images alone, and not delta radiomics features (contrary to the analysis of the cluster response). Delta radiomics could potentially yield better discrimination, and to do this, one would require an earlier interval MR imaging midway through treatment, so that the prediction model could expedite a go-no-go decision regarding treatment continuation. Thirdly, the candidate clinical factors related to the RN response to bevacizumab were determined based on clinical experience and prior studies [33,34]. There might be

other important clinical factors that could augment the results of the clinical model. Fourthly, we focused exclusively on a single type of textural features (GLCM). The incorporation of other radiomics features holds the potential for further enhancing the performance of our radiomics model.

5. Conclusion

Overall, our radiomics approach yielded intralesional resolution, enabling a more refined feature selection process for predicting bevacizumab efficacy in the treatment of RN. We anticipate that this method will be considerably more valuable in clinical settings for evaluating heterogeneous lesions compared to conventional radiomics techniques.

CRediT authorship contribution statement

Study conception and design: **Hong Qi Tan**, **Melvin L.K. Chua**, **Yamei Tang**. Patient recruitment, Data acquisition and analysis: **Jinhua Cai**, **Luo Huang**, **Yamei Tang**. Data interpretation: All authors. Statistical analyses: **Jinhua Cai**, **Shi Hui Tay**. Obtained funding: **Melvin L.K. Chua**, **Yamei Tang**. Administrative, technical, or material support: **Jinhua Cai**, **Melvin L.K. Chua**, **Yamei Tang**. Study supervision: **Melvin L.K. Chua**, **Yamei Tang**. Drafting of manuscript: **Hong Qi Tan**, **Jinhua Cai**, **Shi Hui Tay**, **Melvin L.K. Chua**, **Yamei Tang**. Approval of final manuscript: All authors.

Declaration of Competing Interest

The authors declare no direct conflict of interests. Melvin L.K. Chua reports personal fees from Astellas, Janssen, Bayer, Pfizer, MSD, Varian, Telix Pharmaceuticals, personal fees and non-financial support from AstraZeneca, personal fees and grants from Ferring, non-financial support from Decipher Biosciences, non-financial support from MedLever, consults for immunoSCAPE Inc., and is a co-inventor and co-owns the patent of a High Sensitivity Lateral Flow Immunoassay For Detection of Analyte in Sample (10202107837T), Singapore, outside the submitted work.

Data availability

Data generated or analyzed during the study are available from the corresponding author upon request under the premise of a research collaboration.

Appendix A. Supporting information

Supplementary data associated with this article can be found in the online version at doi:10.1016/j.csbj.2023.11.040.

References

1 Toonkel LM. Advances in radiation therapy for head and neck cancer. Semin Surg Oncol 1991. https://doi.org/10.1002/ssu.2980070109.
2 Grégoire V, Langendijk JA, Nuyts S. Advances in radiotherapy for head and neck cancer. J Clin Oncol 2015. https://doi.org/10.1200/JCO.2015.61.2994.

3 McDonald MW, Liu Y, Moore MG, Johnstone PAS. Acute toxicity in comprehensive head and neck radiation for nasopharynx and paranasal sinus cancers: Cohort comparison of 3D conformal proton therapy and intensity modulated radiation therapy. Radiat Oncol 2016. https://doi.org/10.1186/s13014-016-0600-3.

4 Siddiqui F, Movsas B. Management of radiation toxicity in head and neck cancers. Semin Radiat Oncol 2017. https://doi.org/10.1016/j.semradonc.2017.04.008.

5 Van den Bosch L, et al. Comprehensive toxicity risk profiling in radiation therapy for head and neck cancer: a new concept for individually optimised treatment. Radiother Oncol 2021. https://doi.org/10.1016/j.radonc.2021.01.024.

6 Chao ST, et al. Challenges with the diagnosis and treatment of cerebral radiation necrosis. Int J Radiat Oncol Biol Phys 2013;87:449–57.

7 Gupta T, et al. Three-dimensional conformal radiotherapy (3D-CRT) versus intensity modulated radiation therapy (IMRT) in squamous cell carcinoma of the head and neck: a randomized controlled trial. Radiother Oncol 2012. https://doi.org/10.1016/j.radonc.2012.07.001.

8 Gupta T, et al. Intensity-modulated radiation therapy versus three-dimensional conformal radiotherapy in head and neck squamous cell carcinoma: long-term and mature outcomes of a prospective randomized trial. Radiat Oncol 2020. https://doi.org/10.1186/s13014-020-01666-5.

9 Siu A, et al. Radiation necrosis following treatment of high grade glioma-a review of the literature and current understanding. Acta Neurochir 2012;154:191–201.

10 Lee AWM, et al. Clinical diagnosis of late temporal lobe necrosis following radiation therapy for nasopharyngeal carcinoma. Cancer 1988;61:1535–42.

11 Xu Y, et al. Bevacizumab monotherapy reduces radiation-induced brain necrosis in nasopharyngeal carcinoma patients: a randomized controlled trial. Int J Radiat Oncol Biol Phys 2018;101:1087–95.

12 Argiris A, et al. Phase II randomized trial of radiation therapy, cetuximab, and pemetrexed with or without bevacizumab in patients with locally advanced head and neck cancer. Ann Oncol 2016. https://doi.org/10.1093/annonc/mdw204.

13 Vial A, et al. The role of deep learning and radiomic feature extraction in cancer-specific predictive modelling: a review. Transl Cancer Res 2018;7:803–16.

14 Gillies RJ, Kinahan PE, Hricak H. Radiomics: images are more than pictures, they are data. Radiology 2016;278:563–77.

15 Afshar, P., Mohammadi, A., Plataniotis, K.N., Oikonomou, A. & Benali, H. From hand-crafted to deep learning-based cancer radiomics: Challenges and opportunities. *arXiv* (2018).

16 Cai J, et al. A radiomics model for predicting the response to bevacizumab in brain necrosis after radiotherapy. Clin Cancer Res 2020. https://doi.org/10.1158/1078-0432.CCR-20-1264.

17 Chen X, Ren L, Qiu G, Cao L. Long-term recurrence and brain metastasis of nasopharyngeal carcinoma mimicking cystic radiation encephalopathy relapse: a case report. BMC Neurol 2021. https://doi.org/10.1186/s12883-021-02088-w.

18 Zaffino P, Raudaschl P, Fritscher K, Sharp GC, Spadea MF. Technical note: plastimatch mabs, an open source tool for automatic image segmentation. Med Phys 2016;43:5155–60.

19 Guo P, et al. Improved variable selection algorithm using a LASSO-Type penalty, with an application to assessing hepatitis b infection relevant factors in community residents. PLoS One 2015;10:e0134151.

20 Zwanenburg A, et al. The image biomarker standardization initiative: standardized quantitative radiomics for high-throughput image-based phenotyping. Radiology 2020. https://doi.org/10.1148/radiol.2020191145.

21 Hancer E, Xue B, Zhang M. A survey on feature selection approaches for clustering. Artif Intell Rev 2020;53:4519–45.

22 Dash, M. & Liu, H. Feature selection for clustering. in Lecture Notes in Computer Science (including subseries Lecture Notes in Artificial Intelligence and Lecture Notes in Bioinformatics) (eds. T., T., H., L. & ALP, C.) vol. 1805 110–121 (Springer, 2000).

23 Şenbabaoğlu Y, Michailidis G, Li JZ. Critical limitations of consensus clustering in class discovery. Sci Rep 2014;4:6207.

24 Lambin P, et al. Radiomics: the bridge between medical imaging and personalized medicine. Nat Rev Clin Oncol 2017. https://doi.org/10.1038/nrclinonc.2017.141.

25 Bera K, Braman N, Gupta A, Velcheti V, Madabhushi A. Predicting cancer outcomes with radiomics and artificial intelligence in radiology. Nat Rev Clin Oncol 2022. https://doi.org/10.1038/s41571-021-00560-7.

26 Li YQ, Tan JSH, Wee JTS, Chua MLK. Adaptive radiotherapy for head and neck cancers: fact or fallacy to improve therapeutic ratio. Cancer Radiother 2018. https://doi.org/10.1016/j.canrad.2018.01.003.

27 Zhuang H, Shi S, Yuan Z, Chang JY. Bevacizumab treatment for radiation brain necrosis: mechanism, efficacy and issues. Mol Cancer 2019. https://doi.org/10.1186/s12943-019-0950-1.

28 Liao G, et al. Bevacizumab treatment of radiation-induced brain necrosis: a systematic review. Front Oncol 2021. https://doi.org/10.3389/fonc.2021.593449.

29 Wang Y, et al. Reversal of cerebral radiation necrosis with bevacizumab treatment in 17 Chinese patients. Eur J Med Res 2012. https://doi.org/10.1186/2047-783X-17-25.

30 Fave X, et al. Delta-radiomics features for the prediction of patient outcomes in non-small cell lung cancer. Sci Rep 2017. https://doi.org/10.1038/s41598-017-00665-z.

31 Boothe D, et al. Bevacizumab as a treatment for radiation necrosis of brain metastases post stereotactic radiosurgery. Neuro Oncol 2013;15:1257–63.

32 Selvaraju RR, et al. Grad-CAM: visual explanations from deep networks via gradient-based localization. Int J Comput Vis 2020. https://doi.org/10.1007/s11263-019-01228-7.

33 Ruben JD, et al. Cerebral radiation necrosis: incidence, outcomes, and risk factors with emphasis on radiation parameters and chemotherapy. Int J Radiat Oncol Biol Phys 2006. https://doi.org/10.1016/j.ijrobp.2005.12.002.

34 Brandsma D, Stalpers L, Taal W, Sminia P, van den Bent MJ. Clinical features, mechanisms, and management of pseudoprogression in malignant gliomas. Lancet Oncol 2008;9:453–61.